

# Unlocking 3D Affordance Segmentation with 2D Semantic Knowledge

Yu Huang<sup>1</sup>, Zelin Peng<sup>1,†</sup>, Changsong Wen<sup>1</sup>, Xiaokang Yang<sup>1</sup>, and Wei Shen<sup>1(✉)</sup>  
<sup>1</sup>MoE Key Lab of Artificial Intelligence, AI Institute, Shanghai Jiaotong University  
 {yellowfish, zelin.peng, changsong, xkyang, wei.shen}@sjtu.edu.cn

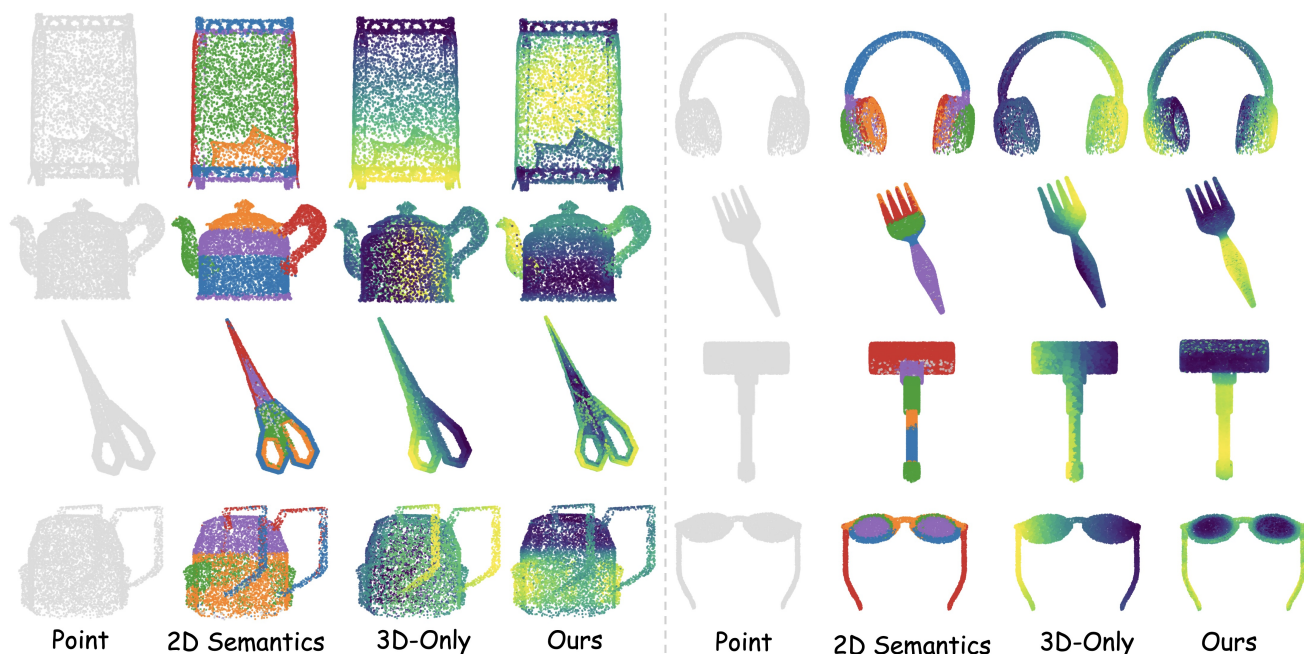


Figure 1. **Qualitative comparison of 3D feature representations.** We visualize learned features across different objects to highlight the semantic organization within 3D representations. The **2D Semantics** column presents clustering results obtained by lifting features from multi-view renderings and encoding them with a 2D Vision Foundation Model (e.g. DINOv3 [36]), which reveal distinct functional regions such as handles and seats. The **3D-Only** column shows features produced solely by a 3D encoder (e.g. PointNet++ [31]), projected into RGB space using PCA, where the boundaries between functional areas remain fuzzy and less coherent. The **Ours** column illustrates our distilled features, which transfer semantic knowledge from 2D models into the 3D domain. Compared to the 3D-only baseline, our method produces features that exhibit stronger semantic organization, clearer separation of functional parts, and more consistent region boundaries across object categories.

## Abstract

Affordance segmentation aims to parse 3D objects into functionally distinct parts, bridging recognition and interaction for applications in robotic manipulation, embodied AI, and AR. While recent studies leverage visual or textual prompts to guide this process, they often rely on point cloud encoders as generic feature extractors, overlooking the intrinsic challenges of 3D data such as sparsity, noise, and geometric ambiguity. As a result, 3D features learned in isola-

tion frequently lack clear and semantically consistent functional boundaries. To address this bottleneck, we propose a semantic-grounded learning paradigm that transfers rich semantic knowledge from large-scale 2D Vision Foundation Models (VFMs) into the 3D domain. Specifically, we introduce Cross-Modal Affinity Transfer (CMAT), a pre-training strategy that aligns a 3D encoder with lifted 2D semantics and jointly optimizes reconstruction, affinity, and diversity to yield semantically organized representations. Building on this backbone, we further design the Cross-modal Affordance Segmentation Transformer (CAST), which integrates multi-modal prompts with CMAT-pretrained features to generate precise, prompt-aware segmentation maps. Extensive experiments on standard benchmarks demonstrate

✉ Corresponding Author: wei.shen@sjtu.edu.cn

† Project Leader.

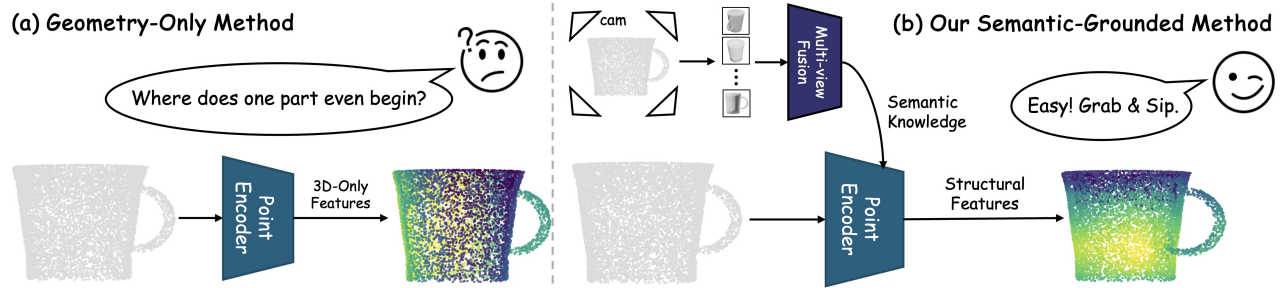


Figure 2. Comparison of Geometry-Only vs. Semantic-Grounded Methods for 3D Representation Learning. (a) A 3D-only encoder produces an unstructured feature space where functional parts are indistinguishable. (b) Our semantic-grounded method leverages knowledge from multi-view 2D images to produce a highly structured feature space, where functional parts like the handle are clearly separated, enabling an intuitive understanding of how to interact with the object.

that our framework establishes new state-of-the-art results for 3D affordance segmentation.

## 1. Introduction

Affordance segmentation, defined as the task of parsing 3D objects into functionally distinct parts such as the seat and legs of a chair, represents a cornerstone in enabling machines to move from passive perception to active interaction. While traditional object recognition merely answers what an object is, affordance segmentation addresses the deeper and more consequential question of how an object can be used. This distinction is fundamental for intelligent systems that must not only recognize their surroundings but also engage with them in meaningful ways. For instance, given a textual prompt such as “Which part of the mug should be grasped to hold it securely?” or a visual prompt showing a hand gripping the mug, an affordance segmentation system should localize the handle as the relevant functional part. By bridging recognition and interaction, affordance segmentation provides the foundation for robotic manipulation [7, 10, 27], embodied AI [25, 52, 53], and imitation learning [8, 15], where success depends not only on identifying objects but also on understanding their actionable possibilities.

Recent advances in affordance segmentation [16, 20, 35, 54] have largely concentrated on leveraging visual or textual prompts to guide the segmentation process. Although these approaches concentrate on multimodal large language models [5, 13, 26, 41] for prompt processing, they typically treat 3D point cloud encoders as generic feature extractors, without directly addressing the intrinsic challenges of 3D data itself, as illustrated in Fig. 2(a). This oversight reveals a critical limitation: geometric information alone is insufficient. Point clouds, due to their sparse sampling and geometrically ambiguous nature, lack the explicit semantic cues necessary to reliably differentiate between functionally distinct

parts. The problem becomes particularly severe in regions that are noisy, incomplete, or locally similar in shape. Consequently, as shown in Fig. 2(a), encoders trained solely on 3D data often struggle to learn features with clear and consistent functional boundaries. This shortcoming remains a fundamental bottleneck for affordance segmentation, a task that inherently relies on precise part-level discrimination.

A promising paradigm [2, 9, 40, 43] to address this limitation is the transfer of rich semantic knowledge from large-scale 2D Vision Foundation Models (VFMs) [3, 29, 32, 36] into the 3D domain. This is achieved by “lifting” features from multi-view 2D images, which provides an effective mechanism for distilling knowledge from pre-trained VFMs such as DINOv3 [36]. As illustrated in the *2D Semantics* column of Fig. 1, the lifted features exhibit clear semantic organization when mapped onto a point cloud, forming distinct clusters that closely correspond to the object’s functionally coherent parts. This observation offers strong evidence that injecting 2D-derived semantic knowledge can effectively guide a 3D encoder to construct a well-structured and semantically discriminative feature space.

Building on this insight, we propose a semantic-grounded learning paradigm for affordance segmentation. As shown in Fig. 2(b), our approach begins by distilling semantic knowledge from a VFM into the 3D domain through multi-view feature lifting, thereby generating dense, per-point semantic structures. To ensure that our 3D encoder effectively internalizes this knowledge, we introduce Cross-Modal Affinity Transfer (CMAT), a novel pre-training strategy that compels the encoder to align with the semantic structures induced by the lifted 2D features. By jointly optimizing three complementary objectives, namely, geometric reconstruction, affinity alignment, and feature diversity, CMAT builds a 3D backbone capable of producing highly structured and discriminative features. Finally, to deploy this pre-trained backbone in practical affordance segmentation tasks, we design the Cross-modal Affordance Seg-

mentation Transformer (CAST), an architecture that fuses CMAT-pretrained 3D features with multi-modal prompts (text or images), thereby generating dense, prompt-aware segmentation maps tailored to specific interaction needs.

In summary, our contributions are threefold:

- We introduce a unified learning paradigm that integrates cross-modal knowledge transfer for pre-training a structurally-aware 3D encoder, followed by fine-tuning for prompt-driven affordance segmentation.
- We propose Cross-Modal Affinity Transfer (CMAT), a pre-training paradigm that distills semantic knowledge from 2D VFMs to supervise a 3D encoder, enabling it to learn structurally superior and semantically organized representations.
- We design the Cross-modal Affordance Segmentation Transformer (CAST), which effectively exploits our pre-trained features and multi-modal prompts to achieve state-of-the-art performance on standard 3D affordance segmentation benchmarks.

## 2. Related Work

**Affordance Segmentation in 3D.** Modern approaches to 3D affordance segmentation [12, 21–23, 49, 50] primarily rely on deep neural networks trained on fully annotated datasets. These methods have become adept at learning the correspondence between local geometric patterns in point clouds and their associated functional labels. However, their performance is fundamentally tied to the quality and scale of 3D supervision, often struggling to generalize to unseen object categories. A core limitation is their reliance on geometric cues alone, which can be ambiguous; for instance, a flat surface could be a “sittable” seat or a “supportable” tabletop, a distinction that requires contextual semantic reasoning beyond local shape.

**Multi-modal Guidance for 3D Segmentation.** To enhance semantic reasoning, a dominant trend [16, 28, 42, 47, 48, 51] is the use of multi-modal guidance, particularly from Vision-Language Models (VLMs) like CLIP [32]. These prompt-driven architectures enable remarkable zero-shot and open-vocabulary segmentation by aligning point cloud features with textual or visual prompts. While these models demonstrate impressive flexibility, their success still depends heavily on the representational quality of the underlying 3D encoder, which may lack fine-grained discriminability to separate functionally distinct parts.

**Knowledge Transfer from 2D VFMs to 3D.** A promising direction for improving 3D representations is transferring semantic knowledge from large-scale 2D Vision Foundation Models (VFMs). A prevalent technique is to lift features from multi-view images extracted by models such as DINO and project them into 3D space, enriching point cloud representations with semantic cues that raw geometry cannot provide. Prior studies show that these lifted features inject

strong semantic signals, helping to impose organization on otherwise ambiguous point clouds and leading to more discriminative feature spaces. However, most existing work focuses on aligning individual features or ensuring broad consistency between 2D and 3D semantics, without explicitly modeling the relational structure among parts, which can leave representations fragmented or inconsistent. Motivated by these limitations, our work explores a semantic-grounded approach that more explicitly structures 3D representations, aiming to achieve finer part-level discrimination required for affordance segmentation.

## 3. Methodology

Our method is structured as a three-stage framework to learn and adapt a 3D representation model with 2D semantic knowledge. The first stage, **Foundational Semantic Grounding**, extracts dense semantic guidance from a pre-trained 2D vision model. The second stage, **Structured Representation Learning**, leverages this guidance to train a 3D point cloud encoder using our *Cross-Modal Affinity Transfer* (CMAT) objective to get structural features. In the final stage, **Prompt-driven Task Adaptation**, the pre-trained backbone is specialized for affordance segmentation tasks using the *Cross-modal Affordance Segmentation Transformer* (CAST) architecture. An overview of the complete framework is shown in Figure 3.

### 3.1. Stage 1: Foundational Semantic Grounding

The effectiveness of our pre-training hinges on a high-quality supervisory signal. This initial stage is dedicated to generating this signal by leveraging the rich representations learned by a large-scale 2D vision model. This approach allows us to transfer high-level semantic knowledge from the well-studied 2D domain to the 3D domain.

The process starts with a large-scale collection of 3D objects, primarily sourced from diverse public datasets like Objaverse [6] and Behavior-1K [11]. To ensure broad semantic coverage, our curated dataset comprises over 10,000 3D models spanning 101 distinct object categories that are commonly found in daily life. These categories range from furniture and kitchenware to tools and electronic appliances, providing a rich and varied foundation for learning generalizable affordance representations. For each 3D point cloud  $P = \{\mathbf{p}_i \in \mathbb{R}^3\}_{i=1}^N$ , we render  $V$  multi-view RGB images. Each image is then passed through a frozen, pre-trained 2D encoder,  $\Phi_{2D}$  (we use DINOv3 [36]), to obtain dense feature maps. Following established lifting techniques [43], these 2D features of multiple views are projected back and interpolated onto the original 3D points. The output of this stage is a set of lifted features per point,  $F^{2D} = \{\mathbf{f}_i^{2D} \in \mathbb{R}^{d_{2D}}\}_{i=1}^N$ . The resulting  $F^{2D}$  is a dense and semantic-grounded feature that can provide the semantic knowledge to guide the next stage’s learning.

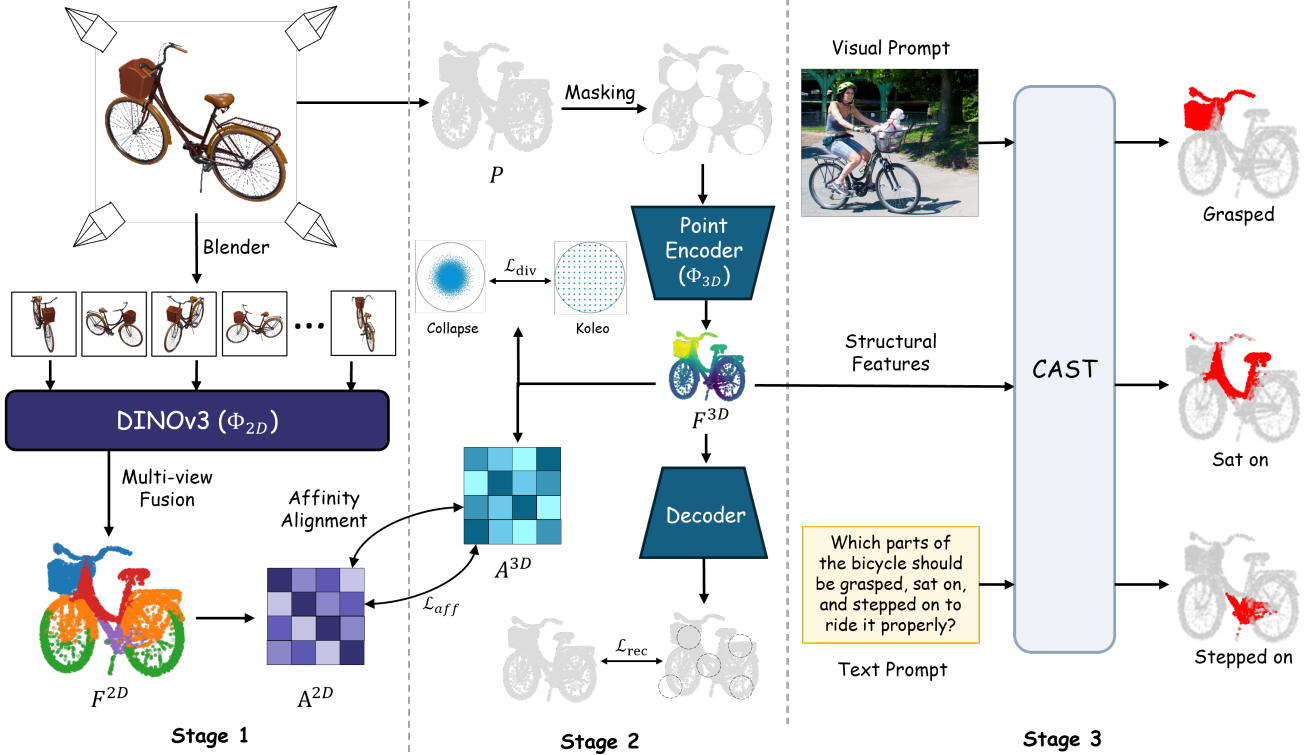


Figure 3. An overview of our three-stage learning framework. In **Stage 2 (Structured Representation Learning)**, we pre-train a 3D backbone ( $\Phi_{3D}$ ) using our proposed **Cross-Modal Affinity Transfer (CMAT)** objective. The training is guided by a combination of three complementary losses: geometric reconstruction, affinity alignment, and feature diversity. In **Stage 3 (Prompt-driven Task Adaptation)**, the resulting structurally-aware backbone is fine-tuned for affordance segmentation. Our **Cross-modal Affordance Segmentation Transformer (CAST)** architecture ingests the pre-trained 3D features and fuses them with a multi-modal prompt (visual or textual) to produce the final segmentation.

### 3.2. Stage 2: Structured Representation Learning

With the semantic knowledge established, this stage focuses on the core pre-training of our 3D backbone,  $\Phi_{3D}$ , to internalize this cross-modal knowledge. Our **Cross-Modal Affinity Transfer (CMAT)** method trains the 3D model to organize its feature space in alignment with the semantic structure provided by the 2D teacher model. The backbone is a PointMAE-style [30] transformer encoder that processes the point cloud as a sequence of patches,  $\mathcal{P} = \{\mathcal{P}_j\}_{j=1}^M$ . For each patch  $\mathcal{P}_j$ , we compute its patch-level 2D semantic feature  $\bar{\mathbf{f}}_j^{2D}$  and 3D feature  $\bar{\mathbf{f}}_j^{3D}$  by average pooling the per-point features:

$$\bar{\mathbf{f}}_j^{2D} = \frac{1}{|\mathcal{P}_j|} \sum_{\mathbf{p}_i \in \mathcal{P}_j} \mathbf{f}_i^{2D}, \quad (1)$$

$$\bar{\mathbf{f}}_j^{3D} = \frac{1}{|\mathcal{P}_j|} \sum_{\mathbf{p}_i \in \mathcal{P}_j} \mathbf{f}_i^{3D}, \quad (2)$$

where  $\mathbf{f}_i^{2D} \in \mathbb{R}^{d_{2D}}$  is the lifted semantic feature from Stage 1 and  $\mathbf{f}_i^{3D} \in \mathbb{R}^{d_{3D}}$  is the output of  $\Phi_{3D}$ .

Based on these patch-level embeddings, we construct

cross-modal affinity matrices that capture the pairwise relational structure of features. Specifically, the *teacher affinity matrix*  $A^{2D} \in \mathbb{R}^{M \times M}$  is defined as

$$A_{jk}^{2D} = \frac{\bar{\mathbf{f}}_j^{2D} \cdot \bar{\mathbf{f}}_k^{2D}}{\|\bar{\mathbf{f}}_j^{2D}\| \|\bar{\mathbf{f}}_k^{2D}\|}, \quad (3)$$

and the *student affinity matrix*  $A^{3D} \in \mathbb{R}^{M \times M}$  is computed analogously from  $\bar{\mathbf{f}}_j^{3D}$ . Both  $A^{2D}$  and  $A^{3D}$  represent semantic part-whole relationships between different patches, but derived from two modalities. Figure 3 illustrates this process, where the lifted 2D features provide a structural prior to guide the 3D encoder.

**Geometric Fidelity.** To ensure the model learns the underlying geometric structure of shapes, we employ a masked autoencoding objective inspired by PointMAE. Specifically, we randomly mask a large portion of the input point patches. The model’s encoder processes only the visible patches to generate a latent representation, which is then fed to a lightweight MLP decoder. The decoder is tasked with predicting the geometric center coordinates of

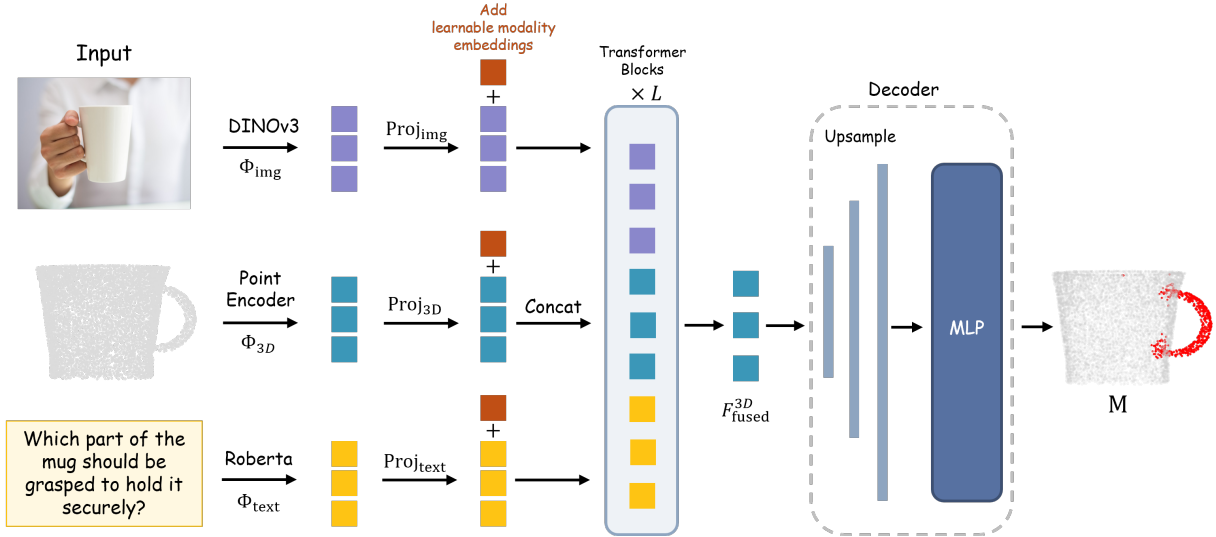


Figure 4. The architecture of our **Cross-modal Affordance Segmentation Transformer (CAST)**. CAST takes geometric patch tokens from our pre-trained 3D backbone and fuses them with multi-modal prompts (text and/or visual). First, all input features are projected into a shared embedding space, and learnable modality embeddings are added to preserve source identity. The geometric and prompt tokens are then concatenated and processed by a stack of co-attentional Transformer blocks. Within this module, self-attention enables deep, bidirectional fusion, allowing the geometric features to become conditioned on the prompt and the prompt to ground itself in the 3D shape. Finally, the updated, prompt-aware patch features are upsampled to the per-point level and processed by a lightweight MLP head to produce the final segmentation mask.

the masked patches. Our *Geometric Reconstruction Loss* ( $\mathcal{L}_{\text{rec}}$ ) is subsequently computed as the Mean Squared Error (MSE) between the predicted centers and the ground-truth centers of these missing patches. This process forces the model to infer the complete shape from partial observations, encouraging it to learn continuous and robust representations that preserve accurate geometric structure.

**Semantic Alignment.** The key to our knowledge transfer is the *Affinity Alignment Loss* ( $\mathcal{L}_{\text{aff}}$ ). By aligning  $A^{3D}$  with the teacher affinity matrix  $A^{2D}$ , the 3D encoder learns to capture semantic relationships that reflect functional structures. Formally:

$$\mathcal{L}_{\text{aff}} = \frac{1}{M^2} \sum_{j=1}^M \sum_{k=1}^M (A_{jk}^{3D} - A_{jk}^{2D})^2. \quad (4)$$

**Representational Expressiveness.** While the semantic alignment and geometric reconstruction losses guide the model towards learning meaningful structures, they do not explicitly prevent the model from collapsing its feature space into a degenerate solution where all patch embeddings are clustered together. To ensure feature diversity and prevent such a collapse, we introduce a *Feature Diversity Loss* ( $\mathcal{L}_{\text{div}}$ ). This loss is implemented using the KoLeo regularizer [34], which is designed to maximize the differential

entropy of the learned embeddings. The intuition is to encourage the set of 3D patch embeddings  $\{\bar{\mathbf{f}}_j^{3D}\}_{j=1}^M$  to span the feature space as uniformly as possible. Specifically, after  $\ell_2$ -normalizing the patch features to constrain them to a unit hypersphere, the loss penalizes small distances between each feature and its nearest neighbor within the set. The objective is formulated as:

$$\mathcal{L}_{\text{div}} = -\frac{1}{M} \sum_{j=1}^M \log(d_j), \quad (5)$$

$$\text{where } d_j = \min_{k \neq j} \|\bar{\mathbf{f}}_j^{3D} - \bar{\mathbf{f}}_k^{3D}\|_2.$$

Minimizing this objective is equivalent to maximizing the nearest-neighbor distances for all patch embeddings, effectively pushing them apart and forcing the model to learn more expressive and discriminative features for different parts of an object.

The overall pre-training objective is a weighted combination of these three components:

$$\mathcal{L}_{\text{pretrain}} = \lambda_{\text{rec}} \mathcal{L}_{\text{rec}} + \lambda_{\text{aff}} \mathcal{L}_{\text{aff}} + \lambda_{\text{div}} \mathcal{L}_{\text{div}}, \quad (6)$$

where the  $\lambda$  hyperparameters balance the objectives of geometric reconstruction, semantic alignment, and feature diversity. This process results in a versatile 3D backbone endowed with a structured semantic understanding, poised for effective downstream application.

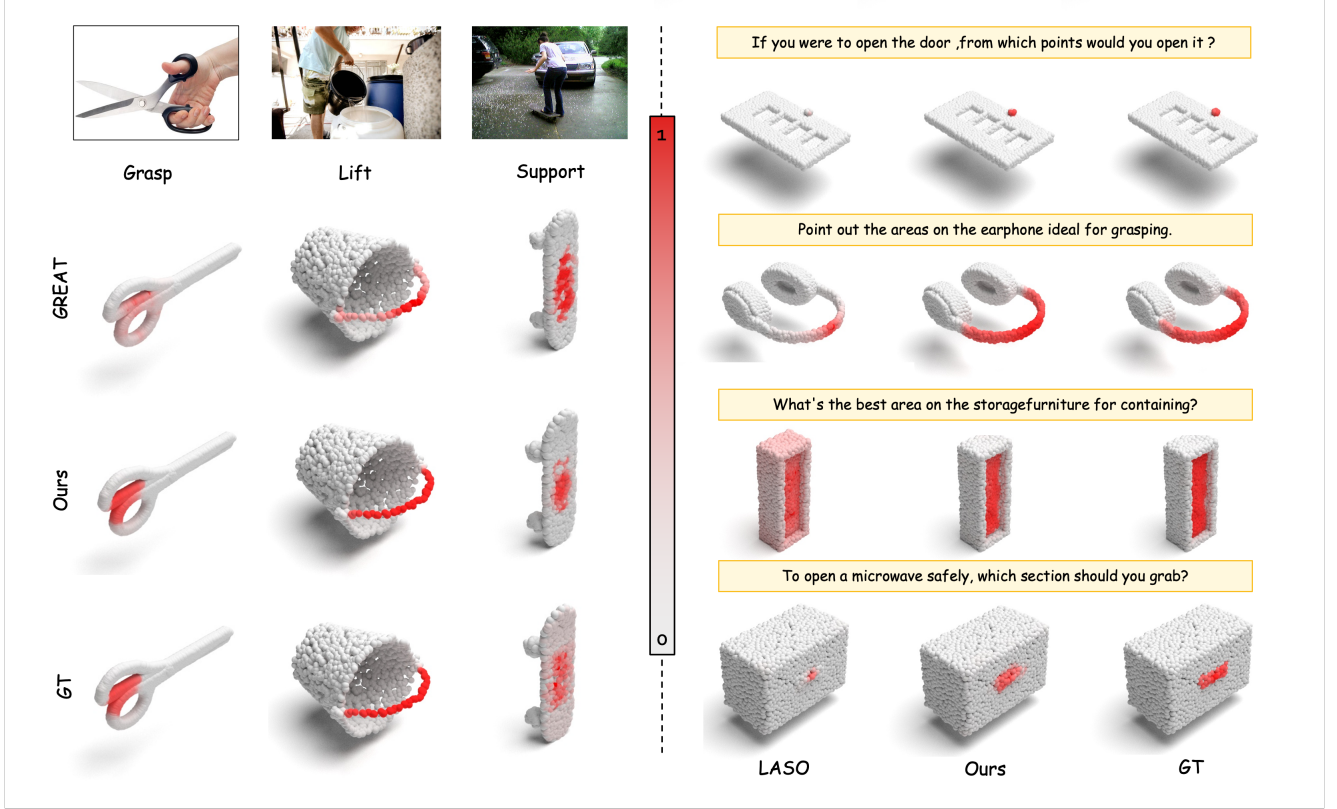


Figure 5. Qualitative comparison on challenging cases from the PIADv2 [35] (visual prompt) and LASO [16] (text prompt) datasets. These examples visually corroborate our quantitative improvements and highlight our framework’s superior fine-grained segmentation capability.

### 3.3. Stage 3: Prompt-driven Task Adaptation

The final stage of our framework specializes this general-purpose backbone for the downstream task of prompt-guided affordance segmentation. For this purpose, we introduce the **Cross-modal Affordance Segmentation Transformer (CAST)**, an architecture designed to seamlessly fuse the learned representations with multimodal prompts.

#### 3.3.1. Architecture for Multi-modal Fusion

The CAST architecture follows a systematic process to integrate multi-modal inputs and generate dense, prompt-aware segmentation masks. It first processes the input point cloud using the pretrained encoder  $\Phi_{3D}$  to obtain a set of geometric patch tokens  $F^{3D}$ .

Currently, user-provided prompts may come from different modalities. A textual phrase (e.g., “handle”) is encoded by  $\Phi_{\text{text}}$  to produce a text feature vector  $\mathbf{f}_{\text{text}}$ , while a visual exemplar is encoded by  $\Phi_{\text{img}}$  to obtain an image feature vector  $\mathbf{f}_{\text{img}}$ . To enable cross-modal interaction, each modality-specific feature is projected into a shared high-dimensional embedding space, with learnable modality em-

beddings added to preserve their source identity.

$$\mathcal{T}_P = \text{Proj}_{3D}(F^{3D}) + \mathbf{E}_{\text{point}}, \quad (7)$$

$$\mathcal{T}_{\text{text}} = \text{Proj}_{\text{text}}(\mathbf{f}_{\text{text}}) + \mathbf{E}_{\text{text}}, \quad (8)$$

$$\mathcal{T}_{\text{img}} = \text{Proj}_{\text{img}}(\mathbf{f}_{\text{img}}) + \mathbf{E}_{\text{img}}. \quad (9)$$

Depending on the input configuration, single or multiple prompt tokens may be present. All available prompt tokens are aggregated into a unified set  $\mathcal{T}_Q = \{\mathcal{T}_{\text{text}}, \mathcal{T}_{\text{img}}\}$ , which is concatenated with the geometric tokens to form the fused sequence  $[\mathcal{T}_Q; \mathcal{T}_P]$ . This sequence is then processed by a stack of  $L$  transformer blocks. Within this co-attentional fusion module, the self-attention mechanism facilitates deep, bidirectional interaction: geometric tokens become conditioned on the prompt(s), and prompts dynamically ground themselves in the 3D geometry.

Finally, to produce a dense prediction, the resulting prompt-conditioned patch features,  $F_{\text{fused}}^{3D}$ , are upsampled back to the original point resolution via a feature propagation module. A lightweight MLP head then maps these per-point features to the final segmentation logits  $M$ .

Table 1. **Quantitative comparison with state-of-the-art methods on the PIAD and PIADv2 datasets.** We report results on both **Seen** and **Unseen** splits. The **best** and second-best results are highlighted. The baseline is our CAST model using frozen encoders from the original PointMAE and DINOv3.

Method	PIAD								PIADv2							
	Seen				Unseen				Seen				Unseen			
	AUC ↑	aIoU ↑	SIM ↑	MAE ↓	AUC ↑	aIoU ↑	SIM ↑	MAE ↓	AUC ↑	aIoU ↑	SIM ↑	MAE ↓	AUC ↑	aIoU ↑	SIM ↑	MAE ↓
<i>State-of-the-art Methods</i>																
MBDF [39]	74.9	9.3	0.415	0.143	58.2	4.2	0.325	0.213	—	—	—	—	—	—	—	—
PMF [38]	75.1	10.1	0.425	0.141	60.3	4.7	0.330	0.211	—	—	—	—	—	—	—	—
FRCNN [46]	76.1	12.0	0.429	0.136	61.9	5.1	0.332	0.195	87.05	33.55	0.600	0.082	72.20	18.08	0.362	0.152
ILN [4]	75.8	11.5	0.427	0.137	59.7	4.7	0.325	0.207	—	—	—	—	—	—	—	—
PFusion [45]	77.5	12.3	0.432	0.135	61.9	5.3	0.330	0.193	—	—	—	—	—	—	—	—
XMF [1]	78.2	12.9	0.441	0.127	62.6	5.7	0.342	0.188	87.39	33.91	0.604	0.078	74.61	17.40	0.361	0.126
IAGNet [47]	84.9	<u>20.5</u>	0.545	<u>0.098</u>	<u>71.8</u>	8.0	0.352	0.127	89.03	34.29	0.623	0.076	73.03	16.78	0.351	<u>0.123</u>
LASO [16]	84.2	19.7	0.590	<b>0.096</b>	69.2	<u>8.0</u>	<u>0.386</u>	<b>0.118</b>	90.34	34.88	0.627	0.077	73.32	16.05	0.354	<u>0.123</u>
GREAT [35]	—	—	—	—	—	—	—	—	<u>91.99</u>	38.03	0.676	<b>0.067</b>	<u>79.57</u>	20.16	0.402	<b>0.109</b>
<i>Our Models</i>																
Baseline	<u>85.5</u>	19.9	<u>0.621</u>	0.105	71.0	7.8	0.379	0.130	91.45	<u>38.16</u>	<u>0.752</u>	0.089	76.87	<u>22.07</u>	<u>0.542</u>	0.142
<b>Ours</b>	<b>88.0</b>	<b>21.4</b>	<b>0.725</b>	0.099	<b>74.8</b>	<b>8.4</b>	<b>0.426</b>	<u>0.125</u>	<b>93.59</b>	<b>45.88</b>	<b>0.783</b>	<u>0.071</u>	<b>83.95</b>	<b>27.40</b>	<b>0.593</b>	0.127

Table 2. The overall results of all comparative methods on the **LASO** dataset. **Seen** and **Unseen** are two partitions of the dataset. Results marked with \* denote the reproduced results, following the data split reported in LASO. AUC and aIOU are shown in percentage. The **best** and 2nd best scores from each metric are highlighted in **bold** and underlined, respectively.

Type	Method	aIoU ↑	AUC ↑	SIM ↑	MAE ↓
Seen	ReferTrans [14]	13.7	79.8	0.497	0.124
	ReLA [17]	15.2	78.9	0.532	0.118
	3D-SPS [24]	11.4	76.2	0.433	0.138
	IAGNet [47]	17.8	82.3	0.561	0.109
	LASO [16]	<u>20.8</u>	<u>87.3</u>	<u>0.629</u>	<b>0.093</b>
	<b>Ours</b>	<b>21.7</b>	<b>88.2</b>	<b>0.681</b>	<u>0.096</u>
Unseen	ReferTrans [14]	10.2	69.1	0.432	0.145
	ReLA [17]	10.7	69.7	0.429	0.144
	3D-SPS [24]	7.9	68.8	0.402	0.158
	IAGNet [47]	12.9	77.8	0.443	0.129
	LASO [16]	14.6	<u>80.2</u>	0.507	0.119
	<b>Ours</b>	<b>17.5</b>	<b>82.9</b>	<b>0.625</b>	<u>0.112</u>

## 4. Experiments

In this section, we conduct a series of experiments to thoroughly evaluate our proposed three-stage framework. We first introduce the experimental setup, including the datasets and evaluation metrics. We then detail our implementation for reproducibility. Subsequently, we present quantitative comparisons against state-of-the-art methods on both visual and text-prompted affordance segmentation tasks. Finally, we perform extensive ablation studies to analyze the contribution of each key component in our framework and showcase qualitative results to provide intuitive insights.

It is important to note that our framework is inherently

designed to process multi-modal prompts, such as a combination of visual cues and textual instructions. However, existing benchmarks for this task are constrained to single-modality inputs, supporting either visual or text prompts but not their concurrent use. To ensure a fair comparison on these datasets, we adapt our model by providing a null input for the modality not supported by the specific benchmark. We posit that the full capabilities of our method will be even more evident on future benchmarks designed for true multi-modal queries, where we expect to see substantial performance gains.

### 4.1. Experimental Setup

**Datasets.** We conduct our evaluation on several established benchmarks for affordance segmentation. We utilize the Point Image Affordance Dataset (PIAD)[47] and its large-scale extension, PIADv2 [35]. PIAD contains 5162 interaction images and 7012 3D objects across 23 categories, while PIADv2 significantly increases this scale to approximately 15213 images and 38889 3D instances spanning 43 object categories. Additionally, we employ the Language-guided Affordance Segmentation on 3D Objects (LASO) dataset [16], which consists of 19751 point-question pairs covering 8434 object shapes. For all datasets, we strictly adhere to their official train/test splits (or Seen/Unseen splits where defined) to ensure fair comparison.

**Evaluation Metrics.** We assess segmentation quality using six metrics. We evaluate performance on average IoU (aIoU) [33], confidence ranking (AUC) [19], shape fidelity

(SIM) [37], and score error (MAE) [44]. This comprehensive suite enables a multi-faceted evaluation beyond simple segmentation overlap.

## 4.2. Implementation Details

**Stage 1: Foundational Semantic Grounding.** The 2D teacher model,  $\Phi_{2D}$ , is a pre-trained DINOv3 with a ViT-Large backbone, with its weights kept frozen throughout the process. For each 3D object in our pre-training dataset, we render  $V = 12$  RGB views at a resolution of  $224 \times 224$ . We extract dense features from the final layer of  $\Phi_{2D}$  and lift them back to the 3D point cloud using an inverse projection and nearest-neighbor interpolation, resulting in the per-point semantic feature set  $F^{2D}$ .

**Stage 2: Structured Representation Learning.** Our 3D backbone,  $\Phi_{3D}$ , is a PointMAE-style transformer encoder with 12 blocks and an embedding dimension of 384. The input point cloud is grouped into 64 patches. For the geometric reconstruction task, we employ a high masking ratio of 60%. The weights for the combined pre-training objective are set to  $\lambda_{\text{rec}} = 1.0$ ,  $\lambda_{\text{aff}} = 0.1$ , and  $\lambda_{\text{div}} = 0.2$ . We pre-train the model for 150 epochs with a batch size of 128 using the AdamW optimizer. The learning rate starts at  $1e-4$  and decays following a cosine schedule with a warmup period of 15 epochs.

**Stage 3: Prompt-driven Task Adaptation.** For prompt encoding, the text encoder  $\Phi_{\text{text}}$  is a pre-trained RoBERTa-base model [18]. The visual prompt encoder  $\Phi_{\text{img}}$  is a pre-trained DINOv3 with a ViT-Base backbone. The weights of both prompt encoders are kept frozen during fine-tuning. The Cross-modal Affordance Segmentation Transformer (CAST) is built with  $L = 6$  co-attentional fusion blocks. All input point clouds for downstream tasks are uniformly sampled to 2048 points. During fine-tuning, we employ a differential learning rate: the pre-trained backbone  $\Phi_{3D}$  uses a lower learning rate of  $1e-5$ , while the newly initialized CAST modules and segmentation head use a higher rate of  $1e-4$ . The weights for the segmentation loss are  $\lambda_{\text{focal}} = 1.0$  and  $\lambda_{\text{dice}} = 1.0$ . Each model is fine-tuned for 100 epochs with a batch size of 16. All three stages are conducted on 4 NVIDIA RTX 3090 GPUs.

## 4.3. Quantitative Results

**Evaluation on PIAD [47] and PIADv2 [35].** As shown in Table 1, our method sets a new state-of-the-art on the visual-prompted PIAD and PIADv2 benchmarks. On PIAD, our model shows particular strength in capturing shape fidelity, achieving a SIM score of 0.725, a 22.9% relative gain over the previous best. This strong performance is magnified on the more challenging PIADv2 dataset, where

our model surpasses the prior top aIoU score by a substantial 7.85 points on the Seen split and 5.33 points on the Unseen split.

**Evaluation on LASO.** For language-driven segmentation on the LASO dataset (Table 2), our framework again achieves state-of-the-art results. It surpasses the previous best aIoU on both Seen and Unseen splits, reaching new top scores of 21.7% and 17.5%, respectively. This demonstrates our model’s robust ability to ground textual commands onto 3D geometry, validating the effectiveness of our Cross-modal Affordance Segmentation Transformer (CAST).

## 4.4. Ablation Studies

To validate our design choices, we conduct ablation studies on the PIADv2 Seen split, with results in Table 3. Our analysis of the Stage 2 pre-training objective shows that while a geometric reconstruction baseline ( $\mathcal{L}_{\text{rec}}$ ) achieves 39.27% aIoU, incorporating our core affinity alignment loss ( $\mathcal{L}_{\text{aff}}$ ) provides the most significant boost to 44.50%. The full objective, including feature diversity ( $\mathcal{L}_{\text{div}}$ ), reaches our peak performance of 45.88%. We also find that a stronger 2D teacher (DINOv3 over DINOv2) yields a 2.18-point gain. For the downstream architecture, we verify that PointMAE (38.16%) is a more effective backbone than PointNet++ (37.50%) when trained from scratch. Crucially, our full model with Stage 2 pre-training surpasses this non-pre-trained PointMAE baseline by a substantial margin (45.88% vs. 38.16%), demonstrating the profound effectiveness of our CMAT strategy.

Table 3. **Ablation studies on the PIADv2 Seen split.** We analyze Stage 2 pre-training components and Stage 3 backbone choices.

Configuration	aIoU (%) $\uparrow$
<b>Stage 2: Pre-training Objective (on PointMAE with DINOv3 Teacher)</b>	
(1) $\mathcal{L}_{\text{rec}}$ only	39.27
(2) $\mathcal{L}_{\text{rec}} + \mathcal{L}_{\text{aff}}$	44.50
(3) Full Objective ( $\mathcal{L}_{\text{rec}} + \mathcal{L}_{\text{aff}} + \mathcal{L}_{\text{div}}$ )	<b>45.88</b>
(4) Full Objective (Replacing DINOv3 with DINOv2)	43.70
<b>Stage 3: CAST Backbone Choices</b>	
(5) PointNet++ Backbone	37.91
(6) PointMAE Backbone	38.16

## 4.5. Qualitative Analysis

In Figure 5, we provide qualitative results for challenging cases from the PIADv2 and LASO datasets. These visualizations compare our method’s predictions against the ground truth and a strong baseline. For instance, given a visual prompt of a hand holding the scissors, our model accurately segments the very part of handle geometry while the baseline is confused with fine-grained details. Similarly, for the text prompt “open the door” for the door handle, our method correctly identifies the entire part precisely, demonstrating a nuanced understanding of semantic function to a

very small part of the whole object. These examples visually corroborate our quantitative improvements and highlight the superior fine-grained segmentation capability fostered by our framework.

## 5. Conclusion

In this work, we address the inherent semantic ambiguity of 3D point clouds by proposing a novel paradigm that grounds 3D representations in the rich knowledge of 2D Vision Foundation Models. Our method is centered on a Cross-Modal Affinity Transfer (CMAT) pre-training strategy, which teaches a 3D encoder to learn a structurally superior feature space, later adapted for downstream tasks by our Cross-modal Affordance Segmentation Transformer (CAST). Our approach achieves state-of-the-art performance, with comprehensive ablations confirming that these significant gains are directly attributable to our CMAT strategy's effective transfer of relational knowledge across modalities. Ultimately, this work presents a generalizable and powerful paradigm for injecting 2D semantic knowledge into 3D feature learning, holding significant promise for a wide range of future 3D understanding tasks.

## References

- [1] Emanuele Aiello, Diego Valsesia, and Enrico Magli. Cross-modal learning for image-guided point cloud shape completion. In *Advances in Neural Information Processing Systems*, 2022. 7
- [2] Sergio Arnaud, Paul McVay, Ada Martin, Arjun Majumdar, Krishna Murthy Jatavallabhula, Phillip Thomas, Ruslan Partsey, Daniel Dugas, Abha Gejji, Alexander Sax, Vincent-Pierre Berges, Mikael Henaff, Ayush Jain, Ang Cao, Ishita Prasad, Mrinal Kalakrishnan, Michael Rabbat, Nicolas Ballas, Mido Assran, Oleksandr Maksymets, Aravind Rajeswaran, and Franziska Meier. Locate 3d: Real-world object localization via self-supervised learning in 3d, 2025. 2
- [3] Mathilde Caron, Hugo Touvron, Ishan Misra, Hervé Jégou, Julien Mairal, Piotr Bojanowski, and Armand Joulin. Emerging properties in self-supervised vision transformers, 2021. 2
- [4] Honghua Chen, Zeyong Wei, Yabin Xu, Mingqiang Wei, and Jun Wang. Imlovenet: Misaligned image-supported registration network for low-overlap point cloud pairs, 2022. 7
- [5] Zhe Chen, Weiyun Wang, Hao Tian, Shenglong Ye, Zhangwei Gao, Erfei Cui, Wenwen Tong, Kongzhi Hu, Jiapeng Luo, Zheng Ma, et al. How far are we to gpt-4v? closing the gap to commercial multimodal models with open-source suites. *arXiv preprint arXiv:2404.16821*, 2024. 2
- [6] Matt Deitke, Dustin Schwenk, Jordi Salvador, Luca Weihs, Oscar Michel, Eli VanderBilt, Ludwig Schmidt, Kiana Ehsani, Aniruddha Kembhavi, and Ali Farhadi. Objaverse: A universe of annotated 3d objects. *arXiv preprint arXiv:2212.08051*, 2022. 3
- [7] Wenlong Huang, Chen Wang, Yunzhu Li, Ruohan Zhang, and Li Fei-Fei. Rekep: Spatio-temporal reasoning of relational keypoint constraints for robotic manipulation. *arXiv preprint arXiv:2409.01652*, 2024. 2
- [8] Ahmed Hussein, Mohamed Medhat Gaber, Eyad Elyan, and Chrisina Jayne. Imitation learning: A survey of learning methods. *ACM Comput. Surv.*, 50(2), 2017. 2
- [9] Krishna Murthy Jatavallabhula, Alihusein Kuwajerwala, Qiao Gu, Mohd Omama, Tao Chen, Alaa Maalouf, Shuang Li, Ganesh Iyer, Soroush Saryazdi, Nikhil Keetha, Ayush Tewari, Joshua B. Tenenbaum, Celso Miguel de Melo, Madhava Krishna, Liam Paull, Florian Shkurti, and Antonio Torralba. Conceptfusion: Open-set multimodal 3d mapping, 2023. 2
- [10] Yuxuan Kuang, Junjie Ye, Haoran Geng, Jiageng Mao, Congyue Deng, Leonidas Guibas, He Wang, and Yue Wang. Ram: Retrieval-based affordance transfer for generalizable zero-shot robotic manipulation, 2024. 2
- [11] Chengshu Li, Ruohan Zhang, Josiah Wong, Cem Gokmen, Sanjana Srivastava, Roberto Martín-Martín, Chen Wang, Gabriel Levine, Wensi Ai, Benjamin Martinez, Hang Yin, Michael Lingelbach, Minjune Hwang, Ayano Hiranaka, Sujay Garlanka, Arman Aydin, Sharon Lee, Jiankai Sun, Mona Anvari, Manasi Sharma, Dhruva Bansal, Samuel Hunter, Kyu-Young Kim, Alan Lou, Caleb R Matthews, Ivan Villaverteria, Jerry Huayang Tang, Claire Tang, Fei Xia, Yunzhu Li, Silvio Savarese, Hyowon Gweon, C. Karen Liu, Jiajun Wu, and Li Fei-Fei. Behavior-1k: A human-centered, embodied ai benchmark with 1,000 everyday activities and realistic simulation, 2024. 3
- [12] Gen Li, Deqing Sun, Laura Sevilla-Lara, and Varun Jampani. One-shot open affordance learning with foundation models. In *Proceedings of the IEEE/CVF Conference on Computer Vision and Pattern Recognition*, 2024. 3
- [13] Junnan Li, Dongxu Li, Caiming Xiong, and Steven Hoi. Blip: Bootstrapping language-image pre-training for unified vision-language understanding and generation, 2022. 2
- [14] Muchen Li and Leonid Sigal. Referring transformer: A one-step approach to multi-task visual grounding, 2021. 7
- [15] Puhao Li, Tengyu Liu, Yuyang Li, Muzhi Han, Haoran Geng, Shu Wang, Yixin Zhu, Song-Chun Zhu, and Siyuan Huang. Ag2manip: Learning novel manipulation skills with agent-agnostic visual and action representations. *arXiv preprint arXiv:2404.17521*, 2024. 2
- [16] Y. Li, N. Zhao, J. Xiao, C. Feng, X. Wang, and T. Chua. Laso: Language-guided affordance segmentation on 3d object. In *2024 IEEE/CVF Conference on Computer Vision and Pattern Recognition (CVPR)*, 2024. 2, 3, 6, 7
- [17] Chang Liu, Henghui Ding, and Xudong Jiang. Gres: Generalized referring expression segmentation, 2023. 7
- [18] Yinhan Liu, Myle Ott, Naman Goyal, Jingfei Du, Mandar Joshi, Danqi Chen, Omer Levy, Mike Lewis, Luke Zettlemoyer, and Veselin Stoyanov. Roberta: A robustly optimized bert pretraining approach, 2019. 8
- [19] Jorge M. Lobo, Alberto Jiménez-Valverde, and Raimundo Real. Auc: a misleading measure of the performance of predictive distribution models. *Global Ecology and Biogeography*, 17:145–151, 2008. 7

- [20] Dongyue Lu, Lingdong Kong, Tianxin Huang, and Gim Hee Lee. Geal: Generalizable 3d affordance learning with cross-modal consistency, 2024. 2
- [21] Hongchen Luo, Wei Zhai, Jing Zhang, Yang Cao, and Dacheng Tao. One-shot affordance detection. In *IJCAI*, 2021. 3
- [22] Hongchen Luo, Wei Zhai, Jing Zhang, Yang Cao, and Dacheng Tao. Leverage interactive affinity for affordance learning. In *Proceedings of the IEEE/CVF Conference on Computer Vision and Pattern Recognition (CVPR)*, pages 6809–6819, 2023.
- [23] Hongchen Luo, Wei Zhai, Jing Zhang, Yang Cao, and Dacheng Tao. Learning visual affordance grounding from demonstration videos. *IEEE Transactions on Neural Networks and Learning Systems*, 35(11):16857–16871, 2024. 3
- [24] Junyu Luo, Jiahui Fu, Xianghao Kong, Chen Gao, Haibing Ren, Hao Shen, Huaxia Xia, and Si Liu. 3d-sps: Single-stage 3d visual grounding via referred point progressive selection. In *2022 IEEE/CVF Conference on Computer Vision and Pattern Recognition (CVPR)*, page 16433–16442. IEEE, 2022. 7
- [25] Junyi Ma, Xieyuanli Chen, Wentao Bao, Jingyi Xu, and Hesheng Wang. Madiff: Motion-aware mamba diffusion models for hand trajectory prediction on egocentric videos, 2024. 2
- [26] Jiageng Mao, Yuxi Qian, Junjie Ye, Hang Zhao, and Yue Wang. Gpt-driver: Learning to drive with gpt, 2023. 2
- [27] Bogdan Moldovan, Plinio Moreno, Martijn van Otterlo, José Santos-Victor, and Luc De Raedt. Learning relational affordance models for robots in multi-object manipulation tasks. In *2012 IEEE International Conference on Robotics and Automation*, pages 4373–4378, 2012. 2
- [28] Toan Nguyen, Minh Nhat Vu, An Vuong, Dzung Nguyen, Thieu Vo, Ngan Le, and Anh Nguyen. Open-vocabulary affordance detection in 3d point clouds. 2023. 3
- [29] Maxime Oquab, Timothée Darcet, Théo Moutakanni, Huy Vo, Marc Szafraniec, Vasil Khalidov, Pierre Fernandez, Daniel Haziza, Francisco Massa, Alaaeldin El-Nouby, Mahmoud Assran, Nicolas Ballas, Wojciech Galuba, Russell Howes, Po-Yao Huang, Shang-Wen Li, Ishan Misra, Michael Rabbat, Vasu Sharma, Gabriel Synnaeve, Hu Xu, Hervé Jégou, Julien Mairal, Patrick Labatut, Armand Joulin, and Piotr Bojanowski. Dinov2: Learning robust visual features without supervision, 2024. 2
- [30] Yatian Pang, Wenxiao Wang, Francis E. H. Tay, Wei Liu, Yonghong Tian, and Li Yuan. Masked autoencoders for point cloud self-supervised learning, 2022. 4
- [31] Charles R Qi, Li Yi, Hao Su, and Leonidas J Guibas. Pointnet++: Deep hierarchical feature learning on point sets in a metric space. *arXiv preprint arXiv:1706.02413*, 2017. 1
- [32] Alec Radford, Jong Wook Kim, Chris Hallacy, Aditya Ramesh, Gabriel Goh, Sandhini Agarwal, Girish Sastry, Amanda Askell, Pamela Mishkin, Jack Clark, Gretchen Krueger, and Ilya Sutskever. Learning transferable visual models from natural language supervision, 2021. 2, 3
- [33] Md.Atiqur Rahman and Yang Wang. Optimizing intersection-over-union in deep neural networks for image segmentation. In *International Symposium on Visual Computing*, 2016. 7
- [34] Alexandre Sablayrolles, Matthijs Douze, Cordelia Schmid, and Hervé Jégou. Spreading vectors for similarity search, 2019. 5
- [35] Yawen Shao, Wei Zhai, Yuhang Yang, Hongchen Luo, Yang Cao, and Zheng-Jun Zha. Great: Geometry-intention collaborative inference for open-vocabulary 3d object affordance grounding, 2025. 2, 6, 7, 8
- [36] Oriane Siméoni, Huy V. Vo, Maximilian Seitzer, Federico Baldassarre, Maxime Oquab, Cijo Jose, Vasil Khalidov, Marc Szafraniec, Seungeun Yi, Michaël Ramamonjisoa, Francisco Massa, Daniel Haziza, Luca Wehrstedt, Jianyuan Wang, Timothée Darcet, Théo Moutakanni, Leonel Sentana, Claire Roberts, Andrea Vedaldi, Jamie Tolan, John Brandt, Camille Couprie, Julien Mairal, Hervé Jégou, Patrick Labatut, and Piotr Bojanowski. Dinov3, 2025. 1, 2, 3
- [37] Michael J. Swain and Dana H. Ballard. Color indexing. *International Journal of Computer Vision*, 7:11–32, 1991. 8
- [38] Mingkui Tan, Zhuangwei Zhuang, Sitao Chen, Rong Li, Kui Jia, Qicheng Wang, and Yuanqing Li. Epmf: Efficient perception-aware multi-sensor fusion for 3d semantic segmentation. *IEEE Transactions on Pattern Analysis and Machine Intelligence*, 2024. 7
- [39] Xun Tan, Xingyu Chen, Guowei Zhang, Jishiye Ding, and Xuguang Lan. Mbd-net: Multi-branch deep fusion network for 3d object detection, 2021. 7
- [40] Yihe Tang, Wenlong Huang, Yingke Wang, Chengshu Li, Roy Yuan, Ruohan Zhang, Jiajun Wu, and Li Fei-Fei. Uad: Unsupervised affordance distillation for generalization in robotic manipulation, 2025. 2
- [41] Hugo Touvron, Thibaut Lavril, Gautier Izacard, Xavier Martinet, Marie-Anne Lachaux, Timothée Lacroix, Baptiste Rozière, Naman Goyal, Eric Hambro, Faisal Azhar, Aurelien Rodriguez, Armand Joulin, Edouard Grave, and Guillaume Lample. Llama: Open and efficient foundation language models, 2023. 2
- [42] Tuan Van Vo, Minh Nhat Vu, Baoru Huang, Toan Nguyen, Ngan Le, Thieu Vo, and Anh Nguyen. Open-vocabulary affordance detection using knowledge distillation and text-point correlation. 2024. 3
- [43] Yixuan Wang, Mingtong Zhang, Zhuoran Li, Tarik Kelestemur, Katherine Driggs-Campbell, Jiajun Wu, Li Fei-Fei, and Yunzhu Li. D<sup>3</sup>fields: Dynamic 3d descriptor fields for zero-shot generalizable rearrangement, 2024. 2, 3
- [44] Cort J. Willmott and Kenji Matsuura. Advantages of the mean absolute error (mae) over the root mean square error (rmse) in assessing average model performance. *Climate Research*, 30:79–82, 2005. 8
- [45] Danfei Xu, Dragomir Anguelov, and Ashesh Jain. Pointfusion: Deep sensor fusion for 3d bounding box estimation, 2018. 7
- [46] Xinli Xu, Shaocong Dong, Tingfa Xu, Lihe Ding, Jie Wang, Peng Jiang, Liqiang Song, and Jianan Li. Fusionrcnn: Lidar-camera fusion for two-stage 3d object detection. *arXiv preprint arXiv:2209.10733*, 2022. 7
- [47] Yuhang Yang, Wei Zhai, Hongchen Luo, Yang Cao, Jiebo Luo, and Zheng-Jun Zha. Grounding 3d object affordance from 2d interactions in images. In *Proceedings of the*

*IEEE/CVF International Conference on Computer Vision (ICCV)*, pages 10905–10915, 2023. [3](#), [7](#), [8](#)

- [48] Yuhang Yang, Wei Zhai, Chengfeng Wang, Chengjun Yu, Yang Cao, and Zheng-Jun Zha. Egochoir: Capturing 3d human-object interaction regions from egocentric views. *arXiv preprint arXiv:2405.13659*, 2024. [3](#)
- [49] Wei Zhai, Hongchen Luo, Jing Zhang, Yang Cao, and Dacheng Tao. One-shot object affordance detection in the wild. *arXiv preprint arXiv:2108.03658*, 2021. [3](#)
- [50] Wei Zhai, Pingyu Wu, Kai Zhu, Yang Cao, Feng Wu, and Zheng-Jun Zha. Background activation suppression for weakly supervised object localization and semantic segmentation. *International Journal of Computer Vision*, pages 1–26, 2023. [3](#)
- [51] Wei Zhai, Yang Cao, Jing Zhang, Haiyong Xie, Dacheng Tao, and Zheng-Jun Zha. On exploring multiplicity of primitives and attributes for texture recognition in the wild. *IEEE Transactions on Pattern Analysis and Machine Intelligence*, 46(1):403–420, 2024. [3](#)
- [52] Zichen Zhang, Hongchen Luo, Wei Zhai, Yang Cao, and Yu Kang. Bidirectional progressive transformer for interaction intention anticipation. *arXiv preprint arXiv:2405.05552*, 2024. [2](#)
- [53] Zichen Zhang, Hongchen Luo, Wei Zhai, Yang Cao, and Yu Kang. Pear: Phrase-based hand-object interaction anticipation. *arXiv preprint arXiv:2407.21510*, 2024. [2](#)
- [54] He Zhu, Quyu Kong, Kechun Xu, Xunlong Xia, Bing Deng, Jieping Ye, Rong Xiong, and Yue Wang. Grounding 3d object affordance with language instructions, visual observations and interactions, 2025. [2](#)